UWB Delay Profile Models for Residential and Commercial Indoor Environments

Saeed S. Ghassemzadeh, *Senior Member, IEEE*, Larry J. Greenstein, *Life Fellow, IEEE*, Thorvardur Sveinsson, Aleksandar Kavčić, *Senior Member, IEEE*, and Vahid Tarokh, *Senior Member, IEEE*

***Abstract*—We present models for the ultrawideband (UWB) channel delay profile in indoor environments, based on the processing of two large sets of measured data. Both measurement sets are for a center frequency of 5 GHz, but the bandwidths are very different—1.25 GHz and 6 GHz. We model both line-of-sight (LOS) and nonline-of-sight (NLOS) paths, and do so for both single-family homes and commercial buildings. Also, we consider both the profile at a receiver point, which we call the multipath intensity profile (MIP), and the locally spatially averaged profile, which we call the power delay profile (PDP). For both cases, we find that the profile for NLOS paths can be modeled as a decaying exponential times a noise-like variation with lognormal statistics and that, for LOS paths, the profile has the same form plus a strong component at the minimum delay. The model consists of statistical descriptions of the parameters of these functions, including the effects of transmit–receive (T–R) distance and of variations from building to building. We show simulation results for a few cases to demonstrate that the model accurately predicts key properties of the measured channels, such as the distribution of rms delay spread.**

***Index Terms*—Channel models, delay profiles, delay spread, multipath, ultrawideband.**

I. Introduction

CHARACTERIZING indoor wireless multipath environments has long been a topic of interest, as documented, for example, in [1]–[7]. However, these earlier works were focused on traditional, relatively narrowband systems. With the advent of ultrawideband (UWB) communications, attention has shifted to bandwidths that are not small with respect to the center frequency. Recent efforts have addressed both path loss (e.g., [8] and [9]) and the multipath delay profile, the latter being the focus of our study. Several statistical models for the UWB delay profile have been proposed, both in IEEE 802.15-SG3a standards contributions (02490r1P802–15_SG3a Channel Modeling-Subcommittee-Report-Final.zip), and in published papers (e.g., [10]–[16]). Our aim here is to report on our own modeling efforts using two large databases of indoor UWB measurements.

Manuscript received June 7, 2004; revised January 5, 2005. This work is based on research supported in part by the National Science Foundation under Grant CCR-0118701 and in part by the Alan T. Waterman award under Grant CCR-0139398. Any opinions, findings and conclusions or recommendation expressed in this publication are those of the authors and do not necessary reflect the views of the National Science Foundation. The review of this paper was coordinated by Prof. R. Qiu.

S. S. Ghassemzadeh is with AT&T Labs-Research, Florham Park, NJ 07932 USA (e-mail: saeedg@research.att.com).

L. J. Greenstein is with WINLAB-Rutgers University, Piscataway, NJ 08855 USA.

T. Sveinsson, A. Kavčić, and V. Tarokh are with Division of Engineering and Applied Sciences, Harvard University, Cambridge, MA 02138 USA.

Digital Object Identifier 10.1109/TVT.2005.851379

In particular, we integrate and expand upon the work reported in [14]–[16]. The underlying principle in this work is that the delay profile can be modeled as the product of a decaying exponential and a noise-like term with lognormal statistics. In [14] and [15], the database was derived from measurements over a 1.25-GHz bandwidth centered at 5 GHz and conducted in single-family homes; in [16], the database was derived from measurements from 2–8 GHz (also centered at 5 GHz) and conducted in both homes and commercial buildings.

Section II presents some definitions, including two versions of the multipath delay profile (the profile-at-a-point and the locally averaged profile). Section III describes the measurement approach and the properties of the two databases. Section IV gives the details of the model development, while Section V presents the numerical results and tabulates the model parameters. Section VI tests the derived models by comparing various simulated profile statistics against those obtained directly from the databases.

II. Definitions

Consider a channel centered on frequency f_c and having a bandwidth $W < 2f_c$. From Nyquist sampling theory, the impulse response of a given path in that channel has a complex envelope (referred to f_c) that can be expressed as

$$h(\tau) = W \sum_{i=0}^{\infty} a_i \,\mathrm{sinc}(W(\tau - \tau_i)); \quad \tau_i = i/W \tag{1}$$

where the a_i's are complex, $\mathrm{sinc}(x) = \sin(\pi x)/\pi x$, and we arbitrarily set $\tau = 0$ at the earliest nonzero part of the response. The above equation can be seen as the convolution of $W\,\mathrm{sinc}(W\tau)$ with the impulse sum

$$g(\tau) = \sum_{i=0}^{\infty} a_i \delta(\tau - \tau_i). \tag{2}$$

Now, assume that $h(\tau)$ has a practical delay extent from $\tau = 0$ to $\tau = \tau_{\max}$, i.e., $h(\tau)$ is, for all practical purposes, zero beyond delay $\tau_{\max}$. This permits us to replace the infinite limit in the summations (1) and (2) with $L - 1$, where L is the integer closest to $W\tau_{\max}$. The result is that the impulse response is specified by the L-fold complex set $\{a_i\}$[1].

[1]The discrete sum (2) suggests a set of physical paths (multipath echoes), with delays at i/W. However, this is a mathematical representation only, which flows from sampling theory. The actual paths in the channel can be quite different, e.g., sparser, not uniformly spaced, and so on. It is the uniformly spaced mathematical paths that we model here. The resulting model is good for any channel bandwidth less than or equal to W.

Following convention, we take an approach slightly different from modeling the a_i's. Specifically, we introduce the *path gain* of the channel response, which is the integral of the squared magnitude of $h(\tau)$ divided by the bandwidth, W. The result is

$$G = \sum_{i=0}^{L-1} |a_i|^2 \tag{3}$$

so that $g(\tau)$ can be rewritten as

$$g(\tau) = \sqrt{G} \sum_{i=0}^{L-1} \tilde{a}_i \delta(\tau - \tau_i); \quad \tilde{a}_i = a_i/\sqrt{G}. \tag{4}$$

Now, the channel response is completely determined by the path gain G and the L-fold set $\{a_i\}$. It is customary in the field of channel modeling to partition the channel behavior in this way, so that large-scale effects like path gain can be distinguished from small-scale effects like multipath. Accordingly, we define the power-delay profile

$$p(\tau) = \sum_{i=0}^{L-1} p_i \delta(\tau - \tau_i) \tag{5}$$

where

$$p_i = |\tilde{a}_i|^2 = |a_i|^2 \Big/ \sum_{i=0}^{L-1} |a_i|^2 \tag{6}$$

and the sum of the p_i's is 1. It is further customary to assume that G and $p(\tau)$ are independent, and that the phases of the a_i's are independent and uniformly distributed on $[0, 2\pi)$. In that case, separate models for the path gain and power-delay profile uniquely specify the channel response. We invoke this approach for the UWB channels we have measured, and we report here solely on the modeling of $p(\tau)$. Models for the path gain in the same environments have been reported elsewhere (see [8] and [9]).

We distinguish two versions of the delay profile. The function $p(\tau)$ in (5) corresponds to a receiver at a fixed point. However, $p(\tau)$ can vary as a receiver moves around that point. The profile-at-a-point is what we call the *multipath intensity profile* (MIP); it has also been called the "local power delay profile" [12]. When averaged spatially around a point (say, over a region whose radius is several wavelengths at the center frequency), we call it the *power delay profile* (PDP)[2], which has also been called the "small-scale-averaged power delay profile" [12]. It should be noted that, when the measurement bandwidth, W, is small compared to the center frequency, local spatial variations in power within a bin are caused by phase changes among the echoes received in that bin; when W is comparable to the center frequency (as it is for our 6-GHz data), the variations are more likely caused by echoes changing bins over the averaging region. Whatever the cause, it is valuable to know the local spatial average of the power.

[2]Conceptually, we might regard the PDP as the spatial average of the MIP. However, the rigorous meaning of each amplitude in the PDP is that it is the same as (6) but with each term $|a_i|^2$ replaced by its spatial average, this differs from taking the spatial average of $|\tilde{a}_i|^2$.

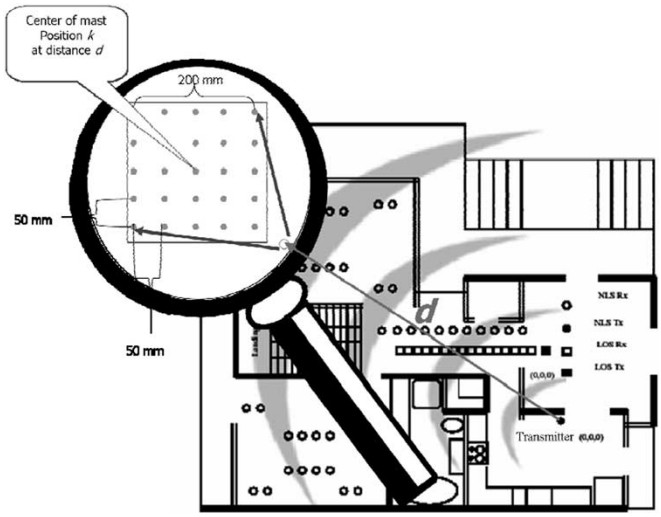

Fig. 1. Illustration of the spatial measurement setup in a typical residence.

We shall present models for both the MIP and PDP and compare them. For either case, we define the *rms delay spread*, τ_{rms}, to be the second central moment (or standard deviation) of the delay profile. We will obtain statistics for this important channel parameter, among others, in comparing our models with the measurement databases.

III. Measurement Approach and Databases

A. Measurements

In each environment measured, whether residential or commercial, a transmitter position was established, and a number of receiver positions were selected spanning a range of distances from the transmitter. Both line-of-sight (LOS) and nonline-of-sight (NLOS) paths were measured, in roughly equal numbers. Fig. 1 shows a layout of transmitter site and receiver locations for one particular environment.

For each transmit-receive path considered, a vector network analyzer (VNA) was used to measure and record the complex frequency response over a bandwidth W centered on 5 GHz. The data record for each record consisted of L complex tone responses, with a tone spacing of W/L. By means of later off-line processing, these frequency response samples were inverse-Fourier-transformed to produce L complex samples (spaced by $1/W$) of the impulse response, representing the a_i's in (2) and (3). Then, using straightforward normalization, the a_i's were converted to $\tilde{a}_i$'s, (6), and the sets $\{|\tilde{a}_i|^2\}$ over all paths in all buildings were used to model the UWB delay profile.

For all measurements, omnidirectional wideband antennas were used at both ends of the link, and the transmissions were vertically polarized. In some cases, measurements were made at just one point per receiver position; in others, a specially constructed metallic grid was used to measure at 25 horizontally-spaced points around the nominal receiver position. This grid is illustrated at the upper left in Fig. 1. The distance between spatial points was 5 cm, corresponding to almost a full-

wavelength at 5 GHz. The spatial measurements were used to obtain the spatially averaged delay profile we call the PDP. Further details on the measurement equipment and technique are in [8] and [9].

B. Databases and Reductions

The features of the two large databases we collected are summarized as follows.

Database 1: These data were collected in 23 single-family dwellings in different parts of New Jersey. The measurement bandwidth was $W = 1.25$ GHz, with $L = 401$ tones. The inverse Fourier transform of the measured set of tones has 401 delay samples spaced by 0.8 ns, with a maximum observable delay of 320 ns. This is well beyond the total delay spread of impulse responses measured in these environments.

In each home, measurements were made for transmit-receive distances ranging from 1 to 10 or 15 meters. The number of LOS and NLOS paths per home was about 15 each, yielding a total of about 700 profiles. For each transmit-receive path, the measurement was made for a single point only, meaning that only MIP's were modeled for this database. At the same time, each measurement was repeated a few hundred times over a 1.8-min interval, to establish temporal variations in these environments. These variations were found to be negligible (see [8] and [14]).

Database 2: These data were collected in 20 homes and for 20 unique transmitter locations within a number of commercial buildings. For both types of buildings, the locations were both in New Jersey and around Boston, MA. (Some of the homes were the same as homes used in Database 1, but for different transmitter locations.) The bandwidth was expanded to 6 GHz (frequencies from 2 to 8 GHz), with $L = 1601$ tones. The resulting impulse responses have 1601 samples spaced by 0.167 ns, with a total span of 267 ns (see [9] and [16]).

In each building, the measurements were made at distances ranging from 0.8 m to 11 m, with about 30 LOS and 30 NLOS paths each. The total number of paths recorded was thus about 2400. In this database, 25 measurements were made in a 25 cm $\times$ 25 cm area at each receiver position, using the grid described above. We were thus able to produce both MIPs (corresponding to the center grid position) and PDPs (corresponding to spatial averages over the 25 grid positions).

In processing each delay profile, we set a threshold and all points below that threshold were excluded from processing. The threshold we used was 10 dB above the average noise level. For Database 1, this led to processed sequence lengths of 30 ns (LOS) and 50 ns (NLOS), on the average; for Database 2, the average processed sequence lengths were 23 ns (LOS) and 43 ns (NLOS). The sequence lengths were shorter for Database 2 because the wider bandwidth raised the relative noise level.

With the above two databases, we have been able to determine the sensitivity of the delay profile to 1) bandwidth (1.25 GHz versus 6 GHz); 2) type of path (LOS versus NLOS); 3) type of building (residential versus commercial); and 4) type of spatial averaging (MIP versus PDP). We describe the functional form of the delay profile in the next section, followed by the numerical values of the model parameters.

IV. Model Development

Both the MIP ($p(\tau)$) and the PDP ($\bar{p}(\tau)$) are weighted sums of uniformly spaced impulses, as given by (5) for the MIP. We begin here with the modeling of the MIP, and then proceed to the PDP.

The set $\{p_i\}$ will change from path to path and from building to building. The modeling challenge is two-fold: 1) To obtain a functional form for p_i versus i that is common to all paths in the environment of interest and 2) to characterize statistically the parameters of that function. We do this in the following two subsections, first for NLOS paths and then for LOS paths.

A. MIP Function for NLOS Paths

Our data reductions show there is a general downward trend of p_i with i, though not quite exponential, as reported in [12], and not usually clustered, as reported in [10]. Exponential models are nearly always "best fits" to data, with a residual variation of data about the fit. In our database, the variations are so strong that we include them in the modeling (analogous to including shadow fading in path loss models). As for clusters, we inspected all our data records visually and found some evidence for them (though at least 70% of all records had only one). In our model, we accommodate clusters as part of the above-mentioned variations. Specifically, we represent the delay profile as the product of a decaying exponential and a noise-like variation, leading to the form

$$p_i = k \cdot s(\tau_i) \cdot \exp[-\tilde{\alpha}(\tau_i/\bar{\tau}_{\rm rms})]; \quad \tau_i/W, \quad i \geq 0 \qquad (7)$$

where

- k normalizing constant, chosen such that p_i sums to 1
- $s(\tau_i)$ noise-like variation with a median of 1 over all delays
- α exponential decay constant (dimensionless)
- $\bar{\tau}_{\rm rms}$ global average of $\tau_{\rm rms}$ over all NLOS paths (computed to be around 8 ns). This normalizing parameter $\bar{\tau}_{\rm rms}$ is used for convenience only.

We have found that the variation $s(\tau_i)$, taken over all paths in all buildings, has the behavior of a log-normal process. In our initial study [14], we treated it as having the same log-normal parameters at all i's, with statistical independence between values at different delays. We subsequently refined that picture, [15], [16], as we describe later.

To see how the function parameters are extracted from data, it is convenient to express (7) in decibels. Thus

$$P_i = K - \alpha(\tau_i/\bar{\tau}_{\rm rms}) + S_i; \quad \text{NLOS Paths} \qquad (8)$$

where $\alpha = (10/\ln 10)\tilde{a}$ and K and S_i are the dB values of k and $s(\tau_i)$, respectively. Since P_i consists of a linear function of τ_i plus a Gauss-like variation, linear regression is an obvious means of fitting the data for a particular measurement. The numbers that come from our data reductions for each record are the squared magnitudes, $p_i = |\tilde{a}_i|^2, i = 0, L-1$ (Section III-A). Creating a scatter plot of P_i versus $\tau_i/\bar{\tau}_{\rm rms}$ (see Fig. 2), one would proceed as follows.

1) Put a linear fit through all the data points, using the method of least squares.

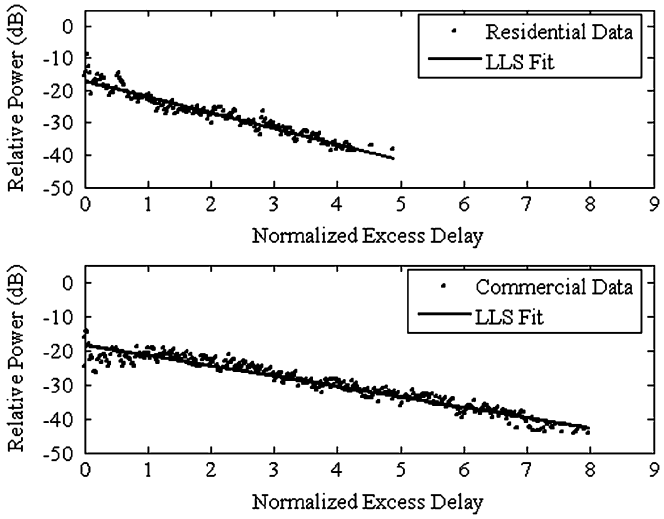

Fig. 2. Scatter plots of P_i versus delay on typical NLOS paths. Each plot is for a particular building in Database 2.

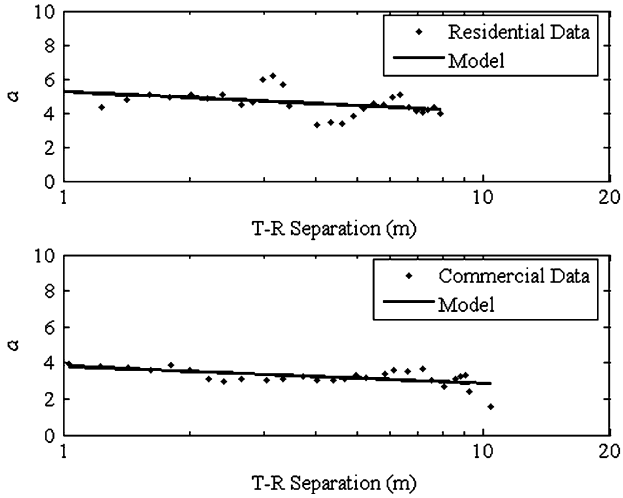

Fig. 3. Scatter plot of α versus distance for typical NLOS paths. Each plot is for a particular building in Database 2.

2) Compute α as the negative of the slope of the straight-line fit.
3) Compute S_i as the deviation of the ith point from the straight-line fit.
4) With $\alpha, \{S_i\}$ and the global quantity $\bar{\tau}_{\rm rms}$ known, convert back to the linear form, (7), and choose k so that the p_i's sum to 1.

Once this procedure is followed for all NLOS paths in all environments, the final step is to model the dependencies and statistics of α and $\{S_i\}$. Before doing so, we consider the LOS case.

B. MIP Function for LOS Paths

The functional form of P_i for LOS paths is the same as for NLOS paths, except that the $i = 0$ term is generally large compared to those that follow it. A suitable representation is therefore

$$P_i = \begin{cases} A; & i = 0 \\ K - \alpha(\tau_i/\bar{\tau}_{\rm rms}) + S_i; & i > 0 \end{cases} \quad \text{LOS Paths} \qquad (9)$$

where A is the LOS component in decibels, and all other parameters are as above. Once the $i = 0$ term is determined and removed from the scatter plot, the procedure for extracting parameter values is the same. The LOS term A must now be added to the list of quantities to be statistically modeled.

C. Modeling α and A

We begin with the intuitive notion that α should be a decreasing function of the transmitter–receiver (T–R) separation, d. This is consistent with the known result that the rms delay spread increases with d [17]. By generating scatter plots of α versus $\log(d)$, we have found the following model to be accurate:

$$\alpha = \alpha_0 - 10\gamma \log_{10} d + \varepsilon; \quad d \text{ in meters} \qquad (10)$$

where α_0 and γ are the intercept and slope, respectively, and ε is a zero-mean Gauss-like variation over d with rms value σ_α. These parameters can be quantified for each building, with separate results for LOS and NLOS paths. Thus, one would form a scatter plot for all NLOS paths, choose (α_0, γ) via least squares fitting so as to minimize the rms ε (yielding σ_α), and then repeat for all LOS paths. By doing this for every building within a category (e.g., residences), the joint distribution of α, γ, and σ_α across that building category can be determined the same way as in [14]. Alternatively, one could pool all data for buildings within a category and find a "global" set, $\{\alpha_0, \gamma, \sigma_\alpha\}$ for each path type, as in [15]. Fig. 3 shows scatter plots of α versus $\log(d)$ for a typical residence and a typical commercial building, derived form processed data in Database 2.

A similar development applies to A. Our data analyses yield the following model:

$$A = A_0 - 10\gamma_A \log_{10} d + \varepsilon_A; \quad d \text{ in meters} \qquad (11)$$

where A_0 and γ_A are the intercept and slope, respectively, and ε_A is a zero-mean Gauss-like variation over d with rms value σ_A. The above comments on parameter extraction apply here. Similarly, the two alternative approaches to data pooling apply here, except that only LOS paths are involved.

D. Modeling $\{S_i\}$

In analyzing the scatter plot of P_i versus i for a given path in a given building, a straight-line fit is chosen for which the set $\{S_i\}$ is zero-mean with minimized variance. We can thus write $S_i = \sigma_s y_i$, where σ_s is the standard deviation of the S_i's and $\{y_i\}$ is a zero-mean set with unit variance. Pooling this set over all NLOS paths in all buildings of Database 1, we obtain the cumulative distribution function (CDF) shown in Fig. 4. The straight line shown connotes a zero-mean, unit-variance Gaussian distribution, and we see that it provides a good fit to the data. Similar results apply to the population of LOS path in Database 1 and to the two path populations (NLOS and LOS) of Database 2.

By forming an *ensemble* of y_i-sequences for each combination of path type and building category, we have learned two

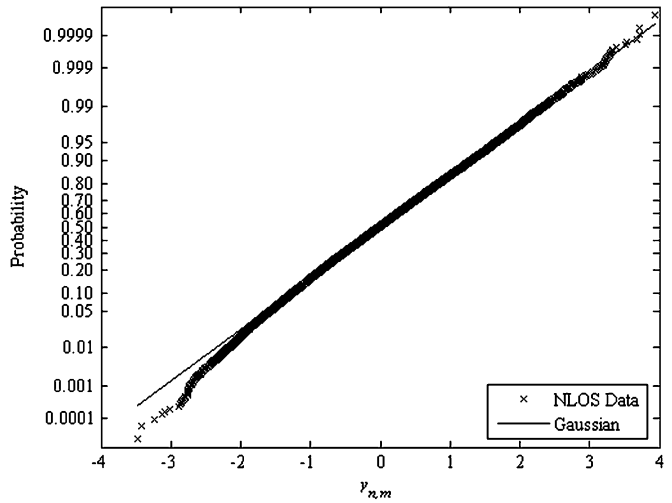

Fig. 4. Cumulative distribution function of normalized deviation y, across buildings and delay, for all NLOS paths in Database 1. The vertical axis is warped such that a straight line connotes a Gaussian distribution.

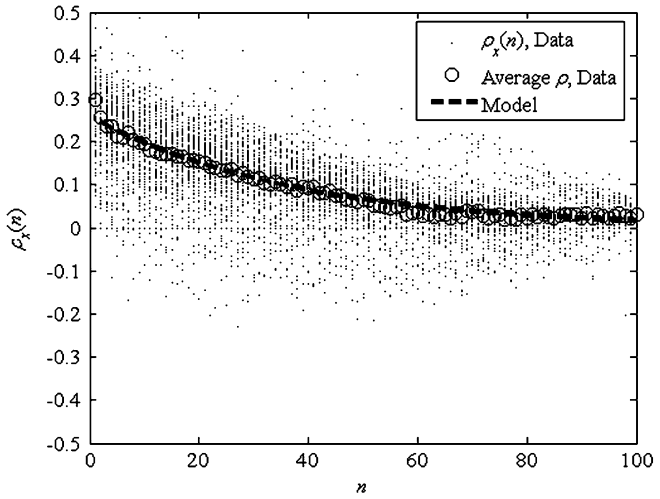

Fig. 5. Inter-multipath correlations ρ_x versus delay, taken over all NLOS paths in Database 1.

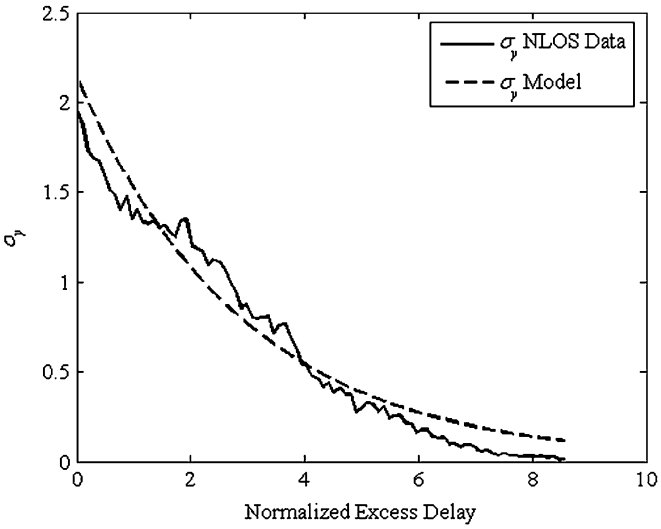

Fig. 6. Standard deviation σ_y versus delay, taken over all NLOS paths in Database 1.

interesting properties of the normalized deviations: 1) there is some correlation among the P_i values at different delays and 2) the mean-square value of y_i, while unity when averaged over i, is larger than 1 at low delays and decays monotonically with delay. It is therefore useful to recast y_i as $y_i = \sigma_y(i)x_i$, where $\{x_i\}$ is a correlated Gaussian sequence with zero mean and unit variance *at every delay*; and $\sigma_y(i)$ is a decaying function of delay.

Based on these observations and our data analyses, we arrived at the following model for S_i :

$$S_i = \sigma_S y_i = \sigma_S \sigma_y(i) x_i \tag{12}$$

$$\sigma_y(i) = \sigma_0 \exp[-\beta(\tau_i/\bar{\tau}_{\rm rms})] \tag{13}$$

$$\rho_x(n) = \begin{cases} 1; & n = 0 \\ a\exp[-b|n|/W\bar{\tau}_{\rm rms}]; & n \neq 0 \end{cases} \tag{14}$$

where $\rho_x(n)$ is the correlation coefficient between two x-values separated by n delay periods. Examples of σ_y versus delay and $\rho_x(n)$ versus delay separation are shown in Figs. 5 and 6, respectively. These figures show both the computed data and the curve fits based on (13) and (14).

Numerical values for σ_0, β, a and b are tabulated later. Generating a Gaussian sequence $\{x_i\}$ having the correlation function in (14) is discussed in the Appendix.

E. Modeling the PDP

Our data analyses show that the same functions that apply to the MIP, i.e., (8) for NLOS paths and (9) for LOS paths, can be used to characterize the spatially averaged MIP, that is, the PDP. Moreover, the models for α, A, and $\{S_i\}$ given above for the MIP apply as well to the PDP. Thus, the MIP and PDP models are the same, but with possibly different parameter values, as we shall see.

V. Numerical Results

We have discussed a large number of cases here, i.e., two databases, two kinds of delay profiles, two types of paths, and two categories of buildings. We have also introduced a large number of model parameters, up to 12 in all for each combination of path type, building category, and delay profile. These can be summarized as follows: parameters $\{\alpha_0, \gamma, \sigma_\alpha\}$ characterize the distance dependence of α; parameters $(A_o, \gamma_A, \sigma_A)$ characterize the distance dependence of A; parameters $(\sigma_s, \sigma_0, \beta)$ characterize the delay dependence of the standard deviation of S_i; parameters (a, b) characterize the correlation between profile amplitudes at different delays; and $\bar{\tau}_{\rm rms}$ is the global average of rms delay spread.

Table I compares three parameter sets for residential environments. One is for the MIP modeling using Database 1 ($W = 1.25$ GHz); another is for MIP modeling using Database 2 ($W = 6$ GHz); and the third is for PDP modeling also

TABLE I
MODEL PARAMETERS FOR RESIDENCES

	Parameter	MIP (W=1.25GHz) LOS	MIP (W=1.25GHz) NLOS	MIP (W=6 GHz) LOS	MIP (W=6 GHz) NLOS	PDP (W=6 GHz) LOS	PDP (W=6 GHz) NLOS
$\alpha(d)$	α_0	2.80	4.60	2.35	3.97	3.51	5.29
	γ	1.40	2.60	0.45	1.62	1.28	2.30
	σ_ε	0.64	0.98	0.73	0.70	1.01	0.84
$A(d)$	A_0	-2.0	NA	-4.13	NA	-4.07	NA
	γ_A	1.10	NA	1.39	NA	1.85	NA
	σ_A	1.20	NA	1.12	NA	0.84	NA
$\rho_x(n)$	a	0.16	0.26	0.29	0.22	0.86	0.73
	b	0.37	0.28	0.20	0.21	0.26	0.151
$\overline{S_i^2(\tau)}$	σ_S	4.70	4.70	4.96	5.10	4.03	3.68
	σ_0	3.0	2.0	2.54	2.44	2.16	1.77
	β	0.43	0.35	0.29	0.33	0.26	0.19
	$\overline{\tau}_{\text{rms}}$, ns	4.54	8.32	3.72	7.39	3.38	7.31

NA – Not applicable

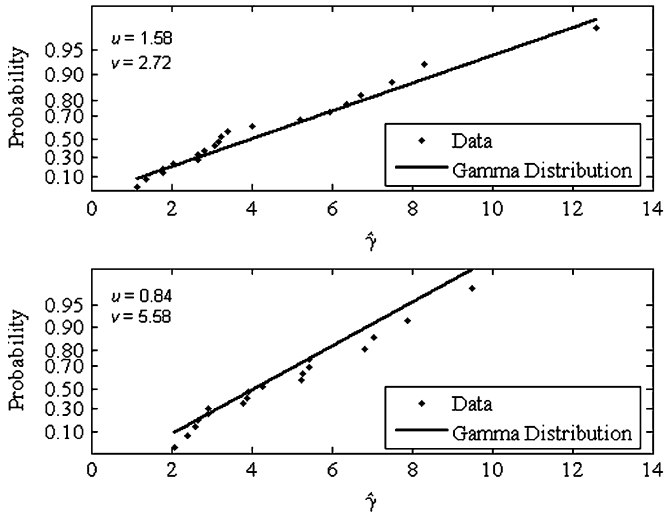

Fig. 7. Cumulative distribution functions of $\hat{\gamma}$ across buildings for all NLOS paths in Database 2. The results are shown for both (top) residential and (bottom) commercial. The vertical axis is warped such that a straight line connotes a Gamma distribution.

using Database 2. The results shown for Database 1 are derived from pooling the MIP samples over all 23 homes. The results for Database 2 are derived by determining the parameters separately for each home and then computing their averages over the 20 homes. What is remarkable about the two columns of MIP parameters is their similarity. This is despite the almost 5 : 1 difference in measurement bandwidth, the different methods of computation, and the different populations of homes. The most significant differences are in the values of A and γ. The 2-dB greater value of A for the narrower-band case is probably due to imperfectly resolving the LOS component, i.e., the $i = 0$ term for that case may be due to multiple returns rather than just one. The discrepancy in γ (the slope of the α versus $\log(d)$ fit) is harder to explain. What we have observed, and show later, is that there is a lot of variability in this slope from one building to another. It may be that the statistics for this parameter do not stabilize in a population of only 20 buildings. In any case, the discrepancy is moderate rather than large.

Comparing the MIP and PDP columns for Database 2, we again see mostly similarities. The most visible discrepancies are in the value of a, which is the correlation coefficient between deviations (S_i) at closely spaced delays; and in the value of σ_s, which is the rms value of the deviations over delay. The smaller value of σ_s for the PDP can be explained as an effect of spatial averaging. The larger a for the PDP is also explainable in terms of spatial averaging, although other factors may also be present. This is an open issue.

Finally, we examine the statistics of the model parameters computed for Database 2. Table II summarizes these results for the set of 20 residences, and Table III does the same for the 20 commercial environments. In each table, LOS and NLOS results are given for both the MIP and PDP, and the data given for each parameter are the mean and standard deviation over the 20 values derived.

Comparing the tables, we see some differences between residential and commercial environments, but few dramatic ones. We also note that, in most cases, the standard deviation across buildings is small. The major exception in both of the above statements pertains to γ. We conclude that the final version of the delay profile model can use the tabulated means of all parameters except γ. For this parameter, we find that a Gamma distribution [18] across buildings provides a good match to data, namely

$$p(\hat{\gamma}) = \frac{1}{u^v \Gamma(v)} \hat{\gamma}^{v-1} \exp(-\hat{\gamma}/u); \quad \hat{\gamma} = \gamma + 2$$
$$\Gamma(v+1) = \int_0^\infty y^v e^{-y} dy; \quad v > -1 \tag{15}$$

where $\Gamma()$ is the gamma function, and u and v are (positive) fitting parameters. Fig. 7 shows the CDF's of $\hat{\gamma}$ for both residential and commercial environments, where the ordinate is warped such that a straight line connotes a gamma distribution.

We can now consolidate our findings into a final version of the delay models.

For both the MIP and the PDP, the formula for the ith amplitude is the same, and is given by (8) and (9) for NLOS and LOS paths, respectively.

The models for α, A, and $\{S_i\}$ are those given in Sections III-C and III-D.

The parameters of these models are the mean values given in Tables II and III, except for γ.

For the parameter γ, (15) applies, with the values of u and v given in Table IV.

All other proposed model parameters are listed in Table IV as well. We note that the parameters chosen are all derived from the reductions of Database 2. This is because of the similarities of results between the two databases (see Table I), and the fact that Database 2 is larger and wider-band. Accordingly, all of the parameters in Table IV, excluding u and v, are repeats of the mean values listed in Tables II and III. We restate them here in order to display all the model parameters in one place.

TABLE II
STATISTICS OF MODEL PARAMETERS (RESIDENTIAL BUILDINGS, W = 6 GHz)

		LOS MIP		NLOS MIP		LOS PDP		NLOS PDP	
Set	Parameter	Mean	Std	Mean	Std	Mean	Std	Mean	Std
$\alpha(d)$	α_0	2.35	0.86	3.97	1.15	3.51	1.49	5.29	2.02
	γ	0.45	1.06	1.62	1.69	1.28	1.72	2.30	2.88
	σ_ε	0.73	0.40	0.70	0.45	1.01	0.58	0.84	0.59
$A(d)$	A_0	-4.13	1.16	NA	NA	-4.07	1.23	NA	NA
	γ_A	1.39	1.55	NA	NA	1.35	1.71	NA	NA
	σ_A	1.12	0.25	NA	NA	0.84	0.22	NA	NA
$\rho_x(n)$	a	0.29	0.19	0.22	0.07	0.86	0.33	0.73	0.11
	b	0.20	0.10	0.21	0.06	0.19	0.08	0.15	0.04
$\overline{S_i^2(\tau)}$	σ_S	4.96	0.61	5.10	0.36	4.03	0.95	3.68	0.84
	σ_0	2.54	0.24	2.44	0.43	2.16	0.30	1.77	0.29
	β	0.29	0.09	0.33	0.10	0.26	0.10	0.19	0.07

NA – Not applicable

TABLE III
STATISTICS OF MODEL PARAMETERS (COMMERCIAL BUILDINGS, W = 6 GHz)

		LOS MIP		NLOS MIP		LOS PDP		NLOS PDP	
Set	Parameter	Mean	Std	Mean	Std	Mean	Std	Mean	Std
$\alpha(d)$	α_0	1.99	0.76	3.33	1.15	2.98	1.46	5.13	1.56
	γ	-0.32	0.92	1.58	1.63	-0.22	1.76	2.67	2.09
	σ_ε	0.38	0.19	0.95	1.48	0.47	0.24	0.87	0.63
$A(d)$	A_0	-4.74	1.01	NA	NA	-4.68	0.93	NA	NA
	γ_A	2.45	2.06	NA	NA	2.38	1.97	NA	NA
	σ_A	1.16	0.27	NA	NA	0.88	0.20	NA	NA
$\rho_x(n)$	a	0.11	0.07	0.15	0.06	0.60	0.10	0.54	0.1
	b	0.16	0.06	0.20	0.08	0.21	0.08	0.12	0.05
$\overline{S_i^2(\tau)}$	σ_S	4.41	0.12	4.98	0.17	2.84	0.35	3.25	0.57
	σ_0	2.55	0.25	2.25	0.39	2.10	0.18	1.76	0.34
	β	0.34	0.04	0.31	0.06	0.30	0.06	0.18	0.09

NA – Not applicable

TABLE IV
PROPOSED MODEL PARAMETERS

		Residential MIP		Commercial MIP		Residential PDP		Commercial PDP	
Set	Parameter	LOS	NLOS	LOS	NLOS	LOS	NLOS	LOS	NLOS
$\alpha(d)$	α_0	2.35	3.97	1.99	3.33	3.51	5.29	2.98	5.13
	v	3.92	5.15	5.44	11.89	3.69	2.72	1.53	5.58
	u	0.62	0.70	0.33	0.33	0.89	1.58	1.31	0.84
	σ_ε	0.73	0.70	0.38	0.95	1.01	0.84	0.47	0.87
$A(d)$	A_0	-4.13	NA	-4.74	NA	-4.07	NA	-4.68	NA
	γ_A	1.39	NA	2.45	NA	1.35	NA	2.38	NA
	σ_A	1.12	NA	1.16	NA	0.84	NA	0.88	NA
$\rho_x(n)$	a	0.29	0.22	0.11	0.07	0.86	0.73	0.60	0.54
	b	0.20	0.21	0.16	0.20	0.26	0.15	0.21	0.12
$\overline{S_i^2(\tau)}$	σ_S	4.96	5.10	4.41	4.98	4.03	3.68	2.84	3.25
	σ_0	2.54	2.44	2.55	2.25	2.16	1.77	2.10	1.76
	β	0.29	0.33	0.34	0.31	0.26	0.19	0.30	0.18
	$\overline{\tau}_{\text{rms}}$, ns	3.72	7.39	5.95	7.93	3.38	7.31	5.49	8.15

NA – Not applicable

VI. SIMULATION RESULTS

A useful test of a statistical model is to predict important attributes (e.g., the CDF of the rms delay spread) using the model and to then compare them with the same attributes computed from the database. Accordingly, we generated an ensemble of PDPs for each of the four combinations of building type and path type. In each case, we assumed 20 building scenarios and, for each of these, we considered 30 T–R separations spanning the range 0.8–15 m. We used the probability distribution (15) to randomly obtain a γ for each building scenario. Given that γ,

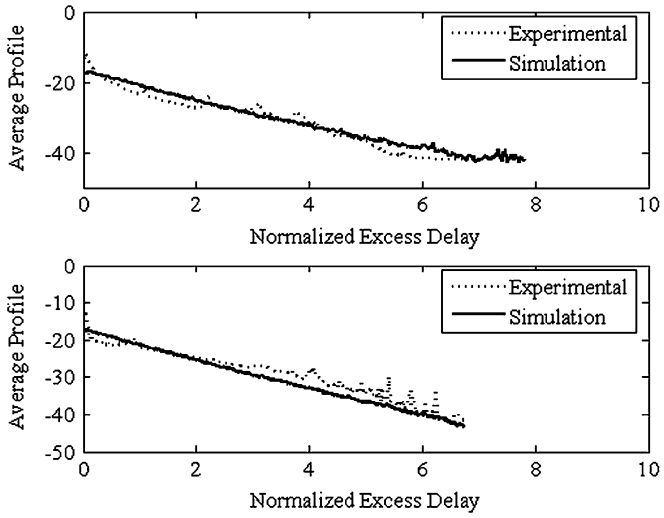

Fig. 8. Average PDP for NLOS paths in Database 2. Results are shown for both (top) residential and (bottom) commercial. For each curve, an average is taken of $p(\tau)$ across the ensemble, and then converted to decibels.

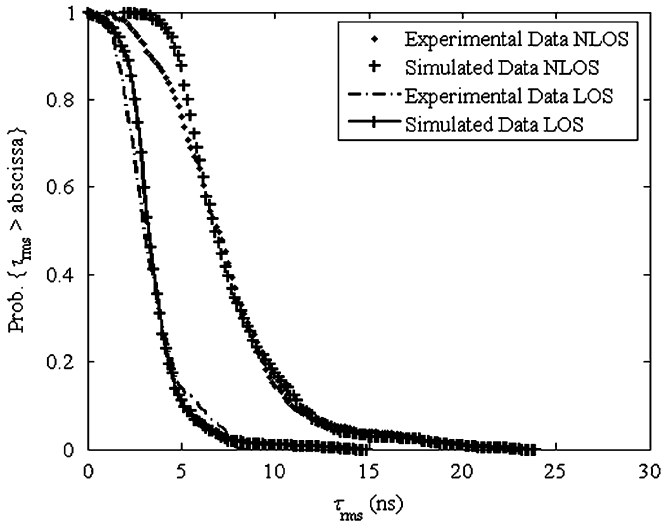

Fig. 9. Cumulative distribution function of rms delay spread in residential buildings in Database 2.

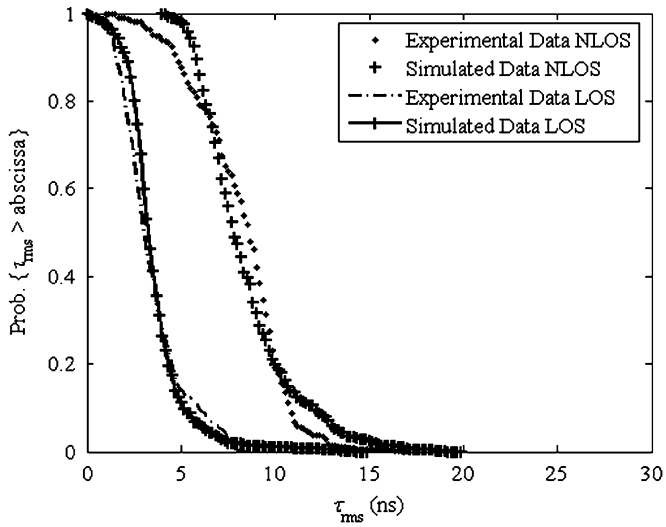

Fig. 10. Cumulative distribution function of rms delay spread in commercial buildings in Database 2.

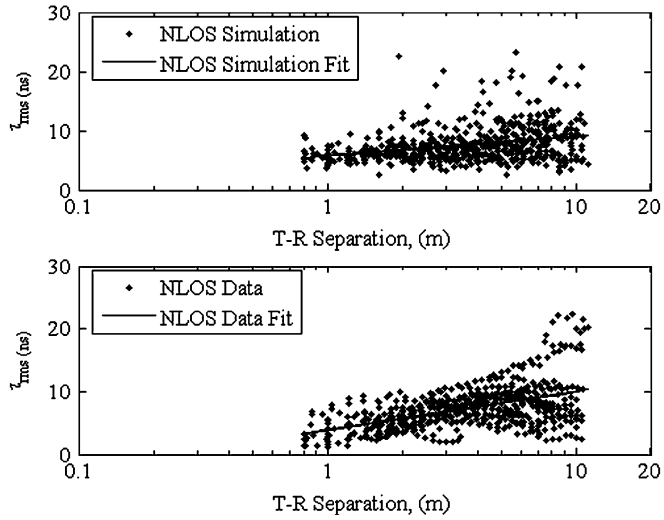

Fig. 11. RMS delay spread versus distance for all residential NLOS paths in Database 2. Results are shown for both (top) simulation and (bottom) measured data.

we simulated a PDP for each of the 30 T–R separations, using the parameter values given in Table IV.

We thus produced a model-derived ensemble of PDPs paralleling the one in Database 2, i.e., one based on the same number of buildings and the same number and range of T–R separations. Computing the mean PDP versus delay across each ensemble, we obtained the comparisons shown in Fig. 8. Computing rms delay spread for each PDP in each ensemble, we obtained CDFs like those shown in Figs. 9 (residences) and 10 (commercial buildings). We also computed scatter plots of rms delay spread versus distance for the two ensembles, and a comparison for NLOS paths is given for residences in Fig. 11; similar results were obtained for commercial buildings. In each comparison, the model performs quite well, i.e., accurately captures the key statistical properties of the channel delay profile.

VII. Conclusion

We have modeled indoor UWB delay profiles for different combinations of building type and path type, both at a point and spatially averaged, and for bandwidths of both 1.25 GHz and 6 GHz. In all cases, the profiles lend themselves to approximation by a decaying exponential times a noise-like lognormal variation, and we have quantified the statistics of these functions. We see mostly minor differences in parameter values between the two bandwidths and between the two kinds of profiles. Further effort is needed to characterize the local spatial statistics of these UWB channels.

APPENDIX

SIMULATION OF $\{X_I\}$

A Gaussian noise sequence $\{x_i\}$ having the correlation function (14) can be realized by passing a white noise sequence through a discrete-time filter. The response of this filter, $G(z)$ can be found by noting that the z-transform of (14) is

$$H(z) = (1-2a) + \frac{a}{1-Cz^{-1}} + \frac{a}{1-Cz} \tag{A1}$$

where

$$C = \exp\{-b/W\bar{\tau}_{\rm rms}\}. \tag{A2}$$

Thus, we need to find $G(z)$ such that $H(z) = G(z)G(1/z)$. To do this, we can rewrite $H(z)$ as

$$H(z) = \frac{A - B(z^{-1}+z)}{(1-Cz^{-1})(1-Cz)} \tag{A3}$$

where

$$A = 1 + C^2(1-2a); \quad B = C(1-a). \tag{A4}$$

Factoring the numerator of (A3), we obtain

$$H(z) = E\frac{(1-Dz^{-1})(1-Dz)}{(1-Cz^{-1})(1-Cz)} \tag{A5}$$

where[3]

$$D = (A - \sqrt{A^2-4B^2})/2B$$
$$E = (A + \sqrt{A^2-4B^2})/2. \tag{A6}$$

The solution for $G(z)$ is therefore

$$G(z) = \sqrt{E}\frac{(1-Dz^{-1})}{(1-Cz^{-1})}. \tag{A7}$$

Passing a white Gaussian noise sequence $\{w_i\}$ through a filter with this transfer function will yield the correlated Gaussian sequence $\{x_i\}$ we seek. The linear difference equation for generating this sequence is

$$x_i = Cx_{i-1} + \sqrt{E}w_i - \sqrt{E}Dw_{i-1} \tag{A8}$$

where C, D, and E are related to a and b in (14) by combining (A2), (A4), and (A6).

ACKNOWLEDGMENT

The authors would like to thank A. Hiamovich and H. Grebel for use of their anechoic chamber at the New Jersey Institute of Technology; C. Rice of AT&T Labs-Research, for valuable comments and suggestions on the hardware setup; and last, but not least, all the homeowners from AT&T Labs and Harvard University who graciously allowed us to invade their premises with our experiments.

[3]There are two solutions for (D, E) that equate (A5) to (A3), and both lead to the same result for ρ_x.

REFERENCES

[1] A. A. Saleh and R. A. Valenzuela, "A statistical model for indoor multipath propagation," *IEEE J. Sel. Areas Commun.*, vol. 5, pp. 128–137, Feb. 1987.

[2] R. J. C. Bultitude, S. A. Mahmoud, and W. A. Sullivan, "A comparison of indoor radio propagation characteristics at 910 MHz and 1.75 GHz," *IEEE J. Select. Areas Commun.*, vol. 7, pp. 20–30, Jan. 1989.

[3] S. J. Howard and K. Pahlavan, "Measurement and analysis of the indoor radio channel in the frequency domain," *IEEE Trans. Instrum. Meas.*, vol. 39, pp. 751–755, Oct. 1990.

[4] T. S. Rappaport, S. Y. Seidel, and K. Takamizawa, "Statistical channel impulse response models for factory and open plan building radio communication system design," *IEEE Trans. Commun.*, vol. 39, pp. 794–806, May 1991.

[5] S. J. Howard and K. Pahlavan, "Autoregressive modeling of wide-band indoor radio propagation," *IEEE Trans. Commun.*, vol. 40, pp. 1540–1552, Sep. 1992.

[6] H. Hashemi, "The indoor propagation channel," in *Proc. IEEE*, vol. 81, Jul. 1993, pp. 943–968.

[7] S. S. Ghassemzadeh, D. L. Schilling, and Z. Hadad, "On the statistics of multipath fading using a direct sequence CDMA signal at 2 GHz," *Int. J. Wireless Inform. Netw.*, Apr. 1994.

[8] S. S. Ghassemzadeh, R. Jana, C. W. Rice, W. Turin, and V. Tarokh, "Measurement and modeling of an indoor UWB channel," *IEEE Trans. Commun.*, vol. 52, pp. 1786–1796, Oct. 2004.

[9] S. S. Ghassemzadeh, L. J. Greenstein, T. Sveinsson, A. Kavčić, and V. Tarokh, "An empirical indoor path loss model for ultra-wideband channels," *J. Commun. Netw.*, Dec. 2003.

[10] A. F. Molisch, J. R. Foerster, and M. Pendergrass, "Channel models for ultra wideband personal area networks," *IEEE Wireless Commun. Mag*, vol. 10, pp. 14–21, Dec. 2003.

[11] M. Z. Win, R. A. Scholtz, and M. A. Barnes, "Ultra-Wide bandwidth signal propagation for indoor wireless communications," in *Proc. IEEE Int. Conf. Commun.*, vol. 1, Jun. 1997, pp. 56–60.

[12] D. Cassioli, M. Z. Win, and A. Molisch, "The ultra-wide bandwidth indoor channel: From statistical model to simulations," *IEEE J. Sel. Areas Commun.*, Aug. 2002.

[13] R. Addler, D. Cheung, E. Green, M. Ho, Q. Li, C. Prettie, L. Rusch, and K. Tinsley, "UWB channel measurements for the home environment," *UWB Intel Forum*, 2001.

[14] S. S. Ghassemzadeh, L. J. Greenstein, T. Sveinsson, and V. Tarokh, "A multipath intensity profile model for residential," in *Proc. IEEE WCNC*, Mar. 2003.

[15] ——, "An impulse response model for residential wireless channels," in *Proc. IEEE Global Commun. Conf.*, vol. 1, Dec. 2003, pp. 1211–1215.

[16] S. S. Ghassemzadeh, L. J. Greenstein, T. Sveinsson, A. Kavčić, and V. Tarokh, "UWB indoor delay profile model for residential and commercial environments," in *IEEE Veh. Technol. Conf.*, vol. 5, Oct. 2003, pp. 3120–3125.

[17] L. J. Greenstein, V. Erceg, Y. S. Yeh, and M. V. Clark, "A new path-gain/delay spread propagation model for digital cellular channels," *IEEE Trans. Veh. Technol.*, vol. 46, no. 2, pp. 477–485, May 1997.

[18] A. Papoulis, *Probability, Random Variables, and Stochastic Processes*. New York, NY: McGraw-Hill, 1991.

Saeed S. Ghassemzadeh (S'88–M'91–SM'02) received the Ph.D. degree in electrical engineering from the City University of New York in 1994.

From 1989 to 1995, he was with InterDigital Communications Corp. as a Principal Research Scientist where he conducted research in the area of propagation channel modeling and spread spectrum access technologies. He joined AT&T Bell-Labs., Whippany, NJ, in 1995 where he was involved in development of CDMA wireless systems. He also conducted research in areas of propagation channel measurement/modeling and satellite access technologies. Currently, he is a Senior Technical Associate in the Communication Technology Research Department, AT&T Labs-Research, Florham Park, NJ. His current research includes wireless channel propagation/modeling, system architecture for increase capacity, performance and range of wireless local area networks, and wireless personal area networks devices.

Dr. Ghassemzadeh is a Member of the IEEE Communication and Vehicular Technology Societies.

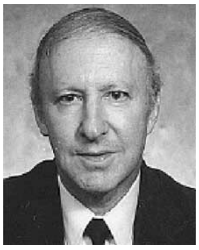

Larry J. Greenstein (M'59–M'67–SM'80–F'87–LF'03) received the B.S., M.S., and Ph.D. degrees in electrical engineering from Illinois Institute of Technology, Chicago, in 1958, 1961, and 1967, respectively.

From 1958 to 1970, he was with IIT Research Institute, Chicago, working on radio frequency interference and anticlutter airborne radar. He joined Bell Laboratories, Holmdel, NJ, in 1970. Over a 32-year AT&T career, he conducted research in digital satellites, point-to-point digital radio, lightwave transmission techniques, and wireless communications. For 21 years during that period (1979–2000), he led a research department renowned for its contributions in these fields. His research interests in wireless communications have included measurement-based channel modeling, microcell system design and analysis, diversity and equalization techniques, and system performance analysis and optimization. He is now a Research Professor at Rutgers WINLAB, Piscataway, NJ, working in the areas of ultrawideband (UWB) techniques, wireless LANs, sensor networks and channel modeling.

Dr. Greenstein has won two best paper awards, and has been a Guest Editor, Senior Editor, and Editorial Board Member for numerous publications. He is currently a Member-at-Large on the IEEE Communications Society's Board of Governors.

Thorvardur Sveinsson received the B.Sc. degree in electrical engineering from the University of Iceland in 2000. In 2003, he received the M.E. degree in electrical engineering from Harvard University, Cambridge, MA.

From 2000 to 2001, he was a Software Engineer at the Icelandic Investment Bank. He is presently working as an Engineer at Kogun Air Defense System, Reykjavik, Iceland.

Aleksandar Kavčić (S'93–M'98–SM'04) received the Dipl.-Ing. degree in electrical engineering from Ruhr University, Bochum, Germany, in 1993, and the Ph.D. degree in electrical and computer engineering from Carnegie Mellon University, Pittsburgh, PA, in 1998.

Since 1998, he has been with the Division of Engineering and Applied Sciences, Harvard University, Cambridge, MA, where he is John L. Loeb Associate Professor of Natural Sciences. From 1998 to 2002, he was an Assistant Professor of electrical engineering at Harvard University. He held short-term research positions at Seagate Technology in 1995, Read-Rite Corporation in 1996, and Quantum Corporation from 1997 to 1998, and has served as a Technical Consultant for Quantum Corporation and Link-A-Media Corporation. His research spans topics in communications, signal processing, information theory and magnetic recording.

Dr. Kavčić received the IBM Partnership Award in 1999 and the NSF CAREER Award in 2000. He served on the Editorial Board of the IEEE Transactions on Information Theory as Associate Editor for Detection and Estimation from 2001 until 2004.

Vahid Tarokh (M'96–SM'02) received the Ph.D. degree in Electrical Engineering from the University of Waterloo, Waterloo, ON, Canada.

He is currently a Perkins Professor of Applied Mathematics and a Hayes Senior Fellow in Electrical Engineering at the Division of Engineering and Applied Sciences of Harvard University, Cambridge, MA.

Dr. Tarokh has been ranked in the list of Top 10 Most Cited Researchers in Computer Science by the ISI Web of Science. He has also received a number of awards including the Gold Medal of the Governor General of Canada 1995, the IEEE Information Theory Society Prize Paper Award 1999, The Alan T. Waterman Award 2001 and was selected as one of the Top 100 Inventors of Years (1999–2002) by the Technology Review Magazine. In 2003, he received an honorary D.Sc. from the University of Windsor.